HHS Public Access

Author manuscript

Nature. Author manuscript; available in PMC 2011 December 23.

Published in final edited form as:

Nature. ; 474(7352): 526–530. doi:10.1038/nature10015.

Tunable pK_a values and the basis of opposite charge selectivities in nicotinic-type receptors

Gisela D. Cymes[1] and **Claudio Grosman**[1]

[1] Department of Molecular and Integrative Physiology, Center for Biophysics and Computational Biology, and Neuroscience Program, University of Illinois at Urbana-Champaign, Urbana, IL 61801, USA

Abstract

Among ion channels, only the nicotinic-receptor superfamily has evolved to generate both cation- and anion-selective members. Although other, structurally unrelated, neurotransmitter-gated cation channels exist, no other type of neurotransmitter-gated anion channel, and thus no other source of fast synaptic inhibitory signals, has been described so far. In addition to the seemingly straightforward electrostatic effect of the presence (in the cation-selective members) or absence (in the anion-selective ones) of a ring of pore-facing carboxylates, mutational studies have identified other features of the amino-acid sequence near the intracellular end of the pore-lining transmembrane segments (M2) that are also required to achieve the high charge selectivity displayed by native channels[1–10]. However, the mechanism underlying this subtler effect has remained elusive[11] and a subject of much speculation. Here, using single-channel electrophysiological recordings to estimate the protonation state of native ionizable side chains, we show that anion-selective type sequences favour, whereas cation-selective type sequences prevent, the protonation of the conserved, buried basic residues at the intracellular entrance of the pore (the M2 0′ position). We conclude that the, previously unrecognized, tunable charge state of the 0′ ring of buried basic side chains is an essential feature of these channels' versatile charge-selectivity filter.

The amino-acid differences that underlie the opposite charge selectivities of the members of the nicotinic-receptor superfamily have been known for several years now [1–10](see Supplementary Fig. 1 and Supplementary Text for a brief introduction to this group of ion channels). Reversal-potential measurements have revealed that the cation-selective members of the superfamily become anion selective upon both, insertion of a proline into the loop that connects transmembrane segments M1 and M2 (between positions −2′ and −1′) and mutation of the pore-lining glutamate at position −1′ to alanine, two changes that bring the

---

Correspondence should be addressed to C.G. 407 S. Goodwin Ave., 524 Burrill Hall, Urbana, IL 61801. grosman@illinois.edu.

Supplementary Information is linked to the online version of the paper at www.nature.com/nature

Author Contributions G.D.C. and C.G. designed experiments, analysed data, and wrote the manuscript; G.D.C performed experiments.

The authors declare no competing financial interests.

sequence of the cation channels closer to that of their anion-selective counterparts (Fig. 1a). Similarly, the reciprocal changes (that is, deletion of the −2′ proline and mutation of the −1′ alanine to glutamate) engineered on (natively) anion-selective members of the superfamily have been shown to confer high selectivity for cations. While the effect of the presence or absence of pore-exposed carboxylates may seem unsurprising, the basis for the effect of the insertion or deletion of a proline from the M1–M2 loop on charge selectivity (Fig. 1b) is much subtler and has remained, largely, a mystery[11].

As a first step toward understanding the effect of the proline insertion, we engineered a proline between positions −2′ and −1′ of the α1, β1 and δ subunits of the (cation-selective) $(\alpha1)_2\beta1\delta\varepsilon$ acetylcholine receptor (muscle AChR), one subunit at a time. Since the ε subunit already has an extra residue at this position (a glycine; Fig. 1a), a proline was introduced in this subunit by a residue-to-residue mutation rather than by insertion. In the presence of a typical, divalent cation-containing solution in the pipette of cell-attached patches ($[Ca^{2+}]$ = 1.8 mM; $[Mg^{2+}]$ = 1.7 mM; solution 1 in Supplementary Table 1), single-channel recordings from the proline-insertion mutant in, for example, the δ subunit display an unusually noisy open-channel level and frequent sojourns of brief duration in the zero-current (‘shut’) level (Fig. 2a; openings are downward deflections). This behaviour, which differs markedly from that of the wild-type channel under identical conditions (Supplementary Fig. 2), strongly hinted at the occurrence of channel block by some of the components of the patch-bathing solutions. Indeed, omission of both Ca^{2+} and Mg^{2+} from the solution in the pipette eliminated this block and, at the same time, uncovered a most unanticipated phenomenon involving two interconverting open-channel conductance levels (Fig. 2a). Unless otherwise indicated, all the results reported here correspond to recordings obtained in the absence of extracellular Ca^{2+} or Mg^{2+}.

As illustrated in Fig. 2b, c, the proline mutation in the four types of AChR subunit leads to the appearance of current fluctuations between two levels of open-channel current with the higher level (the ‘main level’) having roughly the same conductance as the single level observed in the wild-type channel, at least in the case of the δ- and ε-subunit mutants, where the fluctuations were most clearly resolved. Although the conductance of the lower level (the ‘sublevel’) and the occupancy probabilities of the two alternative open-channel states differ among mutants, the underlying phenomenon is undoubtedly the same, as expected from the nearly symmetrical arrangement of the five AChR M2 segments around the channel pore (Supplementary Fig. 3). Moreover, the kinetics of the fluctuations were found to depend on the pH of the external and internal solutions (Fig. 2d) in a manner that is fully consistent with these current oscillations reflecting the alternate protonation and deprotonation of an ionizable side chain. Thus, the effect of these proline mutations on ion conduction is highly reminiscent of the effect of lysine, arginine or histidine substitutions along the M1, M2 or M3 transmembrane segments of the muscle AChR[12,13]; the remarkable difference, however, is that the mutations reported here do not introduce any new protonatable group in the protein’s amino-acid sequence.

To identify the residue(s) responsible for this phenomenon, we mutated each of the (native) ionizable amino acids in and flanking the M2 segment to non-ionizable residues while keeping the extra proline inserted between positions −2′ and −1′. Combining the results of

mutations in the β1 and δ subunits (Fig. 3), we conclude that the observed main-level ⇄ sublevel transitions reflect the protonation and deprotonation of the 0′-lysine side chain of the subunit containing the proline mutation. Furthermore, since protonation reduces the current amplitude (Fig. 2d), we also conclude that AChR mutants having a proline inserted (or substituted) into only one of the five subunits still conduct mostly cations.

A number of observations suggest that the lysines at position 0′ of the different AChR wild-type subunits reside on the stripe of M2 that faces away from the pore's lumen and that their εNH_2 groups are largely deprotonated, even at pH 6.0 (hence, $pK_a<5.0$; Supplementary Text, Supplementary Figs 4 and 5 and Supplementary Table 2). Upon introducing a proline, however, the affinity of these lysines for protons increases, very likely as a result of a rearrangement of the intracellular end of M2. This rearrangement does not appear to be drastic, though, because the extent to which the single-channel conductance is attenuated upon protonation of the 0′ lysines (a measure of the distance between the εNH_3^+ group and the long axis of the pore[12,13]; Supplementary Table 3) does not differ much from that caused by lysines engineered on the back or the sides of M2 (Supplementary Fig. 6) or the front of M1 or M3 (ref. 13). Moreover, albeit higher than in the wild-type AChR, the pK_a values of the 0′-lysine's εNH_3^+ group in the δ- and ε-subunit mutants (~7.58 and ~7.15, respectively; Supplementary Table 3) are still lower than the value expected for this group when fully exposed to bulk water (~10.4) by ~3 units (1 pK_a unit ≈ 1.36 kcal mol^{-1}) which further confirms the notion that these side chains do not face the aqueous lumen of the pore directly. For comparison, the pK_as of lysines engineered on the back of M2 (ref. 12) or on the front of M1 or M3 (ref. 13) are also, at least, ~3 units lower than the bulk-water value of ~10.4 (in Supplementary Table 4, we show that the pK_a values of substituted lysines are rather insensitive to the presence or absence of millimolar concentrations of external Ca^{2+} or Mg^{2+}). In addition, we conclude that the effect of these mutations is not highly position-specific because proline insertions at the five other possible positions along the M1–M2 loop of the δ subunit give rise, essentially, to the same pH-dependent phenotype (Supplementary Fig. 7).

The exact nature of the reorganization of the M1–M2 loop upon mutation, and how this change lowers the hydrophobicity of the microenvironment around the 0′ basic side chain, remains unknown. However, an increased exposure to water (through an increase in solvent penetration and/or a slight repositioning of the side chain) is expected to be an important factor in the stabilization of a positive charge buried in a region of the protein that lacks properly oriented acidic side chains. Indeed, recall from Fig. 3a that the side chains of the nearby −5′ aspartate or the −1′ glutamate do not contribute to the observed main-level ⇄ sublevel current fluctuations neither by being the proton-binding site nor by electrostatically stabilizing the $0'\varepsilon NH_3^+$ group. The idea of a structural rearrangement around position 0′ receives further support from the finding of a complex interaction between the proline mutants and extracellular Ca^{2+} and Mg^{2+} (compare Fig. 2a with Supplementary Fig. 2). Certainly, as elaborated in Supplementary Text, it seems reasonable to ascribe the anomalous nature of this interaction to the likely concomitant rearrangement of the ring of glutamates at the neighbouring position −1′.

Not all of the anion-selective members of the superfamily contain a full ring of 'inserted' prolines at position −2′ of the M1–M2 loop, though. Instead, some β-subunit homomers (such as those formed by the β subunits of $GABA_A$ receptors[14] or of invertebrate GluCl receptors[15]; Fig. 1a) present a full ring of alanines at this position without sacrificing high selectivity for anions. And, even more divergently, some highly anion-selective AChRs from invertebrates do not contain any extra residues in the M1–M2 loop, but rather, replace the −2′ glycine of the cation-selective counterparts with a proline[16] (Fig. 1a). Remarkably, we found that mutating the muscle AChR to mimic the 'atypical' features of these M1–M2 loops also gives rise to current fluctuations that closely resemble those caused by the, more common, proline insertions characterized above. In fact, we found that the insertion or substitution of a number of amino acids (not only proline or alanine) in and around position −2′ have, largely, the same effect (Fig. 4 and Supplementary Text).

Evidently, charge-selective permeation through members of the nicotinic-receptor superfamily has arisen during evolution as a result of several different amino-acid changes in the M1–M2 loop; yet, all these changes seem to act, at least in part, by tuning the proton affinity of the same basic side chain. Consistent with the functional relevance of the different protonation states of the ionizable group at 0′ (neutral in cation-selective members and, at least partly, positively-charged in anion-selective members) we notice that some recently identified cation-selective members of the superfamily from nematodes[17] and bacteria[18] replace this lysine or arginine with non-ionizable residues. However, all known native anion-selective nicotinic-type receptors present a basic residue at position 0′. Whether these additional positive charges are directly responsible for the anion selectivity or, rather, they act to increase the single-channel current amplitude of a channel that is highly selective for anions irrespective of the protonation state of the 0′ basic side chains (as a result, perhaps, of concomitant changes in pore size[6,11,19] or in the orientation of backbone groups[2,10]) remains unclear. What is clear, however, is that both high charge selectivity and high single-channel current amplitude are essential for proper electrical signaling at fast chemical synapses. What is also clear is that the differential tuning of side-chain pK_a values described here represents a novel mechanism for turning protein charges on or off without the need of replacing ionizable amino acids with non-ionizable ones (or *vice versa*).

It is worth noting that the finding of different protonation states for the 0′ basic side chain in cation-selective type *versus* anion-selective type charge-selectivity filters would have gone unnoticed by even such powerful approaches as X-ray or electron crystallography. Certainly, these methods do not typically reach the resolution of 1.0–1.2 Å (especially when applied to membrane proteins) that is needed to detect the presence of hydrogen atoms. Also, although a variety of structure-based computational algorithms for the prediction of protein side-chain pK_a values have been developed and could in principle be applied to structural models of members of the nicotinic-receptor superfamily, their accuracy in the case of large deviations from values in bulk water is still very limited[20–24].

Overall, our results provide a compelling example of the marked sensitivity of side-chain pK_a values to the details of the microenvironment, of the profound impact that differentially tuned proton affinities can have on protein function, and of the advantage evolution has taken of this physicochemical phenomenon. Lastly, our data also remind us that assuming

default protonation states for the ionizable side chains in a protein may be highly misleading, and that the structural determinants of ion-conduction properties through ion channels need not face the lumen of the pore directly.

Methods Summary

Currents were recorded from HEK-293 cells transiently transfected with wild-type or mutant complementary DNAs (cDNAs) encoding for the adult muscle-type AChR (mouse α1, β1, δ and ε subunits) or the α1 GlyR (human or rat isoform b). Single-channel currents were recorded at 22°C from cell-attached patches with the exception of recordings that required access to both sides of the membrane in which case the outside-out configuration with a constant application of ligand was used. Ensemble ('macroscopic') currents were recorded at 22°C from outside-out patches exposed to step changes in the concentration of ligand (solution-exchange time$_{10\text{-}90\%}$<150 μs). The composition of all solutions used for electrophysiological recordings is given in Supplementary Table 1. Extent-of-channel-block and pK_a values were estimated from cell-attached, single-channel recordings as detailed in our previous work[12,13] and in Supplementary Fig. 8. All single-channel current traces are displayed at $f_c \approx$ 6 kHz. Reversal potentials were estimated from macroscopic-current recordings elicited by 1- or 10-ms pulses of ligand applied to outside-out patches (Supplementary Fig. 9). The expression of mutant AChRs in the plasma membrane of transfected cells was estimated using an equilibrium [^{125}I]-α-bungarotoxin binding assay.

Full Methods and any associated references are available in the online version of the paper at www.nature.com/nature.

METHODS

DNA clones, mutagenesis and transfection

HEK-293 cells were transiently transfected with cDNAs encoding for the adult muscle-type AChR (mouse α1, β1, δ and ε subunits) or the α1 GlyR (human or rat isoform b prepared as indicated in ref. 25; no differences were found between the charge selectivities of these two orthologs) using a calcium-phosphate precipitation method. Mutations were engineered using the QuikChange site-directed mutagenesis kit (Stratagene) and were confirmed by dideoxy sequencing. When deemed necessary, mutations that prolong individual activations of the channel ('bursts of openings') were also introduced in the mutant AChR constructs to increase the number of proton-transfer events recorded. These mutations were βV266M (M2 position 13′; ref. 26),δS268Q (M2 12′; ref. 27) or εT264P (M2 12′; ref. 28), and their lack of appreciable effect on charge selectivity and single-channel conductance is shown in Fig. 1b and Supplementary Fig. 10, respectively.

Extent of channel block

Single-channel currents were digitized (at 100 kHz), filtered (cascaded $f_c \approx$ 30 kHz) and idealized (using the SKM algorithm in QuB software[29]) to obtain the mean amplitudes of the different current levels and the sequences of dwell times. *I–V* curves were generated from patch-clamp recordings obtained in the cell-attached configuration, and these only include data on inward currents (Fig. 2c). For most mutants studied here, the rectilinear

portion of the sublevel's *I–V* curve extrapolates onto the voltage axis at a negative potential (whereas the main-level's extrapolates near zero) a likely result of the more pronounced inward rectification of the current sublevel and, for some mutants at least, the result perhaps of the diminished selectivity of the sublevel for cations (note that, under the conditions of our cell-attached experiments, a decrease in cation selectivity would shift the reversal potential to negative values). Because of these different intercepts, the ratio between the sublevel and the main-level single-channel current amplitudes becomes a function of the transmembrane potential, and the choice of any particular voltage value to calculate the extent of channel block from current amplitudes would be arbitrary. Hence, here (as in our previous work; refs 12, 13) we chose to calculate the extent of block using single-channel conductances, instead. As a result, our extent-of-block values differ from those that could be inferred from a mere inspection of the single-channel traces at a single potential (say, −100 mV, in the case of our figures). Different intercepts for the rectilinear portions of the main-level and sublevel *I–V* curves are not unique to the mutants studied here; rather, these differences were also observed for AChR mutants bearing engineered basic residues along M2 (ref. 12). The extent of channel block for each construct was calculated as the difference between the conductance values of the main level and the sublevel normalized by the conductance of the main level. In some cases, the conductance of the main level could not be estimated with confidence (for example, because the open-channel signal dwelled only briefly and infrequently in the main level). In these cases, the normalization was done relative to the conductance of the corresponding background construct (that is, the wild-type AChR with or without one of the burst-prolonging mutations).

pK_a values

Protonation and deprotonation rates (as well as all other transition rates) were estimated from maximum-likelihood fits of single-channel dwell-time sequences with kinetic models (Supplementary Fig. 8) as described in our previous work[12,13]. To this end, we used the MIL algorithm in QuB software[30] with a retrospectively imposed time resolution of 25 μs. The ratio between the proton-dissociation and proton-association rates thus estimated gives the ratio of the probabilities of the engineered ionizable side chain being deprotonated *versus* protonated while the channel is open. The reported pK_a values (Supplementary Tables 3 and 4) were calculated from the product of these ratios and the concentration of protons in the channel-bathing solution (Supplementary Fig. 8). For the calculation of the pK_as of lysine side chains engineered in M1 or M2 (Supplementary Table 4), we used the concentration of protons in the pipette solution of cell-attached patches (that is, pH 6.0 in the case of the mutant at position 11′ and 7.4 in all other cases). For the calculation of the pK_as of the 0′ side chain in the various M1–M2 loop mutants studied here (Supplementary Table 3), however, the choice of a pH value is not obvious because we found that the kinetics of protonation and deprotonation in this region of the channel are sensitive to the pHs of the two solutions bathing the membrane, behaving as if the protonatable group were exposed to a solution of intermediate pH. Hence, although probably not strictly correct, we decided to use a pH of 7.3, a value halfway between the pH of the pipette solution (~7.4) and that of the cytosol (~7.2). This uncertainty leads to a maximum systematic error of ± 0.1 units in the pK_a estimates shown in Supplementary Table 3.

Concentration jumps, reversal potentials and kinetics

Step changes in the concentration of ligand bathing the external aspect of outside-out patches were achieved by the rapid switching of two solutions (differing only in the presence or absence of ligand) flowing from either barrel of a piece of theta-type capillary glass mounted on a piezo-electric device (Burleigh-LSS-3100; Lumen Dynamics) as described previously (solution-exchange $time_{10\text{-}90\%}$<150 μs; ref. 31). Reversal potentials were estimated from *I–V* relationships generated by plotting the peak-current responses to brief (1- or 10-ms) pulses of ligand applied to outside-out patches at concentrations that evoke nearly maximal responses (100 μM ACh for the AChR; 10 mM Gly for the α1 GlyR). Consecutive pulses were separated by 8-s intervals during which the patches were exposed to ligand-free solution and the applied voltage was changed. In these particular experiments, the reference Ag/AgCl wire was connected to the bath solution (the composition of which was the same as that of the solution flowing through the theta-type glass tubing; solution 9 in Supplementary Table 1) through an agar bridge containing 200 mM KCl, to minimize the liquid-junction potential. A new, fresh agar bridge was connected every <2 h. Liquid-junction potentials were calculated using the JPCalc module in pClamp 9.0 (ref. 32). To characterize the kinetics of AChR deactivation, entry into desensitization and recovery from desensitization, and the response to the repetitive application (25 Hz) of nearly-saturating ACh, macroscopic currents were recorded from outside-out patches (at −80 mV) using various 100-μM ACh pulse protocols, as indicated in Supplementary Fig. 5. All macroscopic currents were analyzed using a combination of pClamp 9.0 (Molecular Devices) and SigmaPlot 7.101 (Systat Software) software.

Plasma-membrane AChR expression

To estimate the number of wild-type or mutant AChRs in the plasma membrane, transfected HEK-293 cells were incubated with 20-nM [^{125}I]-α-bungarotoxin (PerkinElmer) in fresh DMEM culture medium at 4–5°C for 2–3 h so as to saturate all toxin-binding sites. The associated radioactivity was measured in a γcounter and was normalized to the corresponding mass of total protein, which was quantified using the bicinchoninic-acid method (Thermo Scientific) after solubilizing the cells with 0.1 N NaOH. The non-specific binding of radiolabeled toxin was estimated on cells transfected with cDNA encoding for the β1, δ and ε subunits of the mouse-muscle AChR (but not the α1 subunit). The amount of [^{125}I]-α-bungarotoxin bound to these mock-transfected cells (normalized to total protein content) was never higher than 6% of that associated with the expression of the wild-type AChR.

Supplementary Material

Refer to Web version on PubMed Central for supplementary material.

Acknowledgments

We thank S. Sine for wild-type muscle AChR cDNA; M. Slaughter and D. Papke for wild-type α1 GlyR cDNA; S. Elenes for critical advice on fast-perfusion experiments; E. Jakobsson and H. Robertson for discussions; and G. Papke, M. Maybaum, J. Pizarek and C. Staehlin for technical assistance. This work was supported by a grant from the US National Institutes of Health (R01-NS042169 to C.G.).

References

1. Galzi JL, et al. Mutations in the ion channel domain of a neuronal nicotinic receptor convert ion selectivity from cationic to anionic. Nature. 1992; 359:500–505. [PubMed: 1383829]
2. Corringer P-J, et al. Mutational analysis of the charge selectivity filter of the α7 nicotinic acetylcholine receptor. Neuron. 1999; 22:831–843. [PubMed: 10230802]
3. Keramidas A, Moorhouse AJ, French CR, Schofield PR, Barry PH. M2 pore mutations convert the glycine receptor channel from being anion- to cation-selective. Biophys J. 2000; 78:247–259. [PubMed: 10866951]
4. Gunthorpe MJ, Lummis SCR. Conversion of the ion selectivity of the 5-HT_{3A} receptor from cationic to anionic reveals a conserved feature of the ligand-gated ion channel superfamily. J Biol Chem. 2001; 276:10977–10983.
5. Jensen ML, et al. The β subunit determines the ion selectivity of the $GABA_A$ receptor. J Biol Chem. 2002; 277:41438–41447. [PubMed: 12177063]
6. Keramidas A, Moorhouse AJ, Pierce KD, Schofield PR, Barry PH. Cation-selective mutations in the M2 domain of the inhibitory glycine receptor channel reveal determinants of ion-charge selectivity. J Gen Physiol. 2002; 119:393–410. [PubMed: 11981020]
7. Thompson AJ, Lummis SCR. A single ring of charged amino acids at one end of the pore can control ion selectivity in the 5-HT_3 receptor. Br J Pharmacol. 2003; 140:359–365. [PubMed: 12970096]
8. Wotring VE, Miller TS, Weiss DS. Mutations at the GABA receptor selectivity filter: a possible role for effective charges. J Physiol. 2003; 548:527–540. [PubMed: 12626678]
9. Menard C, Horvitz HR, Cannon S. Chimeric mutations in the M2 segment of the 5-hydroxytryptamine-gated chloride channel MOD-1 define a minimal determinant of anion/cation permeability. J Biol Chem. 2005; 280:27502–27507. [PubMed: 15878844]
10. Sunesen M, et al. Mechanism of Cl^- selection by a glutamate-gated chloride (GluCl) receptor revealed through mutations in the selectivity filter. J Biol Chem. 2006; 281:14875–14881. [PubMed: 16527818]
11. Keramidas A, Moorhouse AJ, Schofield PR, Barry PH. Ligand-gated ion channels: mechanisms underlying ion selectivity. Prog Biophys Mol Biol. 2004; 86:161–204. [PubMed: 15288758]
12. Cymes GD, Ni Y, Grosman C. Probing ion-channel pores one proton at a time. Nature. 2005; 438:975–980. [PubMed: 16355215]
13. Cymes GD, Grosman C. Pore-opening mechanism of the nicotinic acetylcholine receptor evinced by proton transfer. Nature Struct Mol Biol. 2008; 15:389–396. [PubMed: 18376414]
14. Krishek BJ, Moss SJ, Smart TG. Homomeric β1 γ-aminobutyric $acid_A$ receptor-ion channels: evaluation of pharmacological and physiological properties. Mol Pharmacol. 1996; 49:494–504. [PubMed: 8643089]
15. Cully DF, et al. Cloning of an avermectin-sensitive glutamate-gated chloride channel from *Caenorhabditis elegans*. Nature. 1994; 371:707–711. [PubMed: 7935817]
16. van Nierop P, et al. Identification of molluscan nicotinic acetylcholine receptor (nAChR) subunits involved in formation of cation- and anion-selective nAChRs. J Neurosci. 2005; 25:10617–10626. [PubMed: 16291934]
17. Beg AA, Jorgensen EM. EXP-1 is an excitatory GABA-gated cation channel. Nature Neurosci. 2003; 6:1145–1152. [PubMed: 14555952]
18. Bocquet N, et al. A prokaryotic proton-gated ion channel from the nicotinic acetylcholine receptor family. Nature. 2007; 445:116–119. [PubMed: 17167423]
19. Lee DJ–S, Keramidas A, Moorhouse AJ, Schofield PR, Barry PH. The contribution of proline 250 (P −2′) to pore diameter and ion selectivity in the human glycine receptor channel. Neurosci Lett. 2003; 351:196–200. [PubMed: 14623139]
20. Schutz CN, Warshel A. What are the dielectric 'constants' of proteins and how to validate electrostatic models? Proteins. 2000; 44:400–417. [PubMed: 11484218]
21. Harms MJ, et al. The pK_a values of acidic and basic residues buried at the same internal location in a protein are governed by different factors. J Mol Biol. 2009; 389:34–47. [PubMed: 19324049]

22. Kamerlin SCL, Haranczyk M, Warshel A. Progress in *Ab Initio* QM/MM free-energy simulations of electrostatic energies in proteins: accelerated QM/MM studies of p*K*, redox reactions and solvation free energies. J Phys Chem B. 2009; 113:1253–1272. [PubMed: 19055405]

23. Karp DA, Stahley MR, Garcia-Moreno EB. Conformational consequences of ionization of Lys, Asp, and Glu buried at position 66 in staphylococcal nuclease. Biochemistry. 2010; 49:4138–4146. [PubMed: 20329780]

24. Chimenti MS, Castaneda CA, Majumdar A, Garcia-Moreno EB. Structural origins of high apparent dielectric constants experienced by ionizable groups in the hydrophobic core of a protein. J Mol Biol. 2011; 405:361–377. [PubMed: 21059359]

25. Papke D, Gonzalez-Gutierrez G, Grosman C. Desensitization of neurotransmitter-gated ion channels during high-frequency stimulation: A comparative study of Cys-loop, AMPA and purinergic receptors. J Physiol. 10.1113/jphysiol.2010.203315

26. Engel AG, et al. New mutations in acetylcholine receptor subunit genes reveal heterogeneity in the slow-channel congenital myasthenic syndrome. Hum Mol Genet. 1996; 5:1217–1227. [PubMed: 8872460]

27. Grosman C, Auerbach A. Asymmetric and independent contribution of the second transmembrane segment 12′ residues to diliganded gating of acetylcholine receptor channels. A single-channel study with choline as the agonist. J Gen Physiol. 2000; 115:637–651. [PubMed: 10779320]

28. Ohno K, et al. Congenital myasthenic syndrome caused by prolonged acetylcholine receptor channel openings due to a mutation in the M2 domain of the epsilon subunit. Proc Natl Acad Sci USA. 1995; 92:758–762. [PubMed: 7531341]

29. Qin F. Restoration of single-channel currents using the segmental k-means method based on hidden Markov modeling. Biophys J. 2004; 86:1488–1501. [PubMed: 14990476]

30. Qin F, Auerbach A, Sachs F. Estimating single-channel kinetic parameters from idealized patch-clamp data containing missed events. Biophys J. 1996; 70:264–280. [PubMed: 8770203]

31. Elenes S, Ni Y, Cymes GD, Grosman C. Desensitization contributes to the synaptic response of gain-of-function mutants of the muscle nicotinic receptor. J Gen Physiol. 2006; 128:615–627. [PubMed: 17074980]

32. Barry PH, Lynch JW. Liquid junction potentials and small cell effects in patch- clamp analysis. J Membrane Biol. 1991; 121:101–117. [PubMed: 1715403]

a

		Intracellular end of M1			M1–M2 loop								Intracellular end of M2		
Subunit	Origin	–10′	–9′	–8′	–7′	–6′	–5′	–4′	–3′	–2′	–1′	0′	1′	2′	3′
AChRα1	**mouse**	**F**	**Y**	**L**	**P**	**T**	**D**	**S**	**---**	**G**	**E**	**K**	**M**	**T**	**L**
AChRα1	zebrafish	F	Y	L	P	T	D	S	---	G	E	K	M	T	L
AChRα1	*A. californica*	F	Y	L	P	S	D	S	---	G	E	K	I	T	L
AChRα1	fruit fly	F	Y	L	P	S	D	S	---	G	E	K	I	S	L
AChRα4	mouse	F	Y	L	P	S	E	C	---	G	E	K	V	T	L
AChRα7	mouse	F	L	L	P	A	D	S	---	G	E	K	I	S	L
AChRβ1	**mouse**	**F**	**Y**	**L**	**P**	**P**	**D**	**A**	**---**	**G**	**E**	**K**	**M**	**G**	**L**
AChRδ	**mouse**	**F**	**Y**	**L**	**P**	**G**	**D**	**C**	**---**	**G**	**E**	**K**	**T**	**S**	**V**
AChRε	**mouse**	**Y**	**F**	**L**	**P**	**A**	**Q**	**A**	**G**	**G**	**Q**	**K**	**C**	**T**	**V**
5-HT_{3A}R	mouse	F	C	L	P	P	D	S	---	G	E	R	V	S	F
GlyRα1	mouse	F	W	I	N	M	D	A	A	P	A	R	V	G	L
$GABA_AR$α1	mouse	F	W	L	N	R	E	S	V	P	A	R	T	V	F
GluClα1	*C. elegans*	F	W	F	D	R	T	A	I	P	A	R	V	T	L
HisClα1	fruit fly	F	W	I	K	P	E	A	A	P	A	R	V	T	L
GlyRβ	mouse	F	W	I	N	P	D	A	S	A	A	R	V	P	L
$GABA_AR$β1	mouse	F	W	I	N	Y	D	A	S	A	A	R	V	A	L
GluClβ	*C. elegans*	F	W	I	D	L	H	S	T	A	G	R	V	A	L
AChR B	*L. stagnalis*	F	W	L	P	P	E	S	---	P	A	K	M	Q	L
Capca1_92948	*C. capitata*	F	W	L	P	P	E	S	---	P	A	K	M	M	L
Smp_176310	*S. mansoni*	F	W	L	P	P	E	T	---	P	A	K	M	V	L
AChR2β	*S. haematobium*	F	W	L	P	P	D	S	---	A	A	K	M	M	L
Helro1_192409	*H. robusta*	F	L	L	P	P	D	T	---	N	A	K	I	S	L

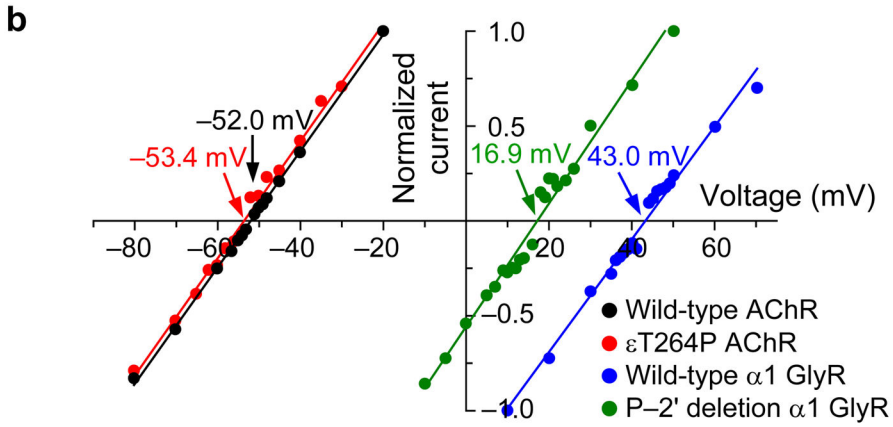

Figure 1. The versatile charge selectivity of nicotinic-type receptors

a, Sequence alignment of residues in and flanking the M1–M2 loop. The broken horizontal line separates the sequences that are known or predicted (on the basis of their sequences) to form cation-selective channels (top) from those that are known or predicted to form anion-selective ones (bottom). Included in this alignment are subunits from receptors to acetylcholine (ACh), serotonin (5-HT), glycine (Gly), γ-aminobutyric acid (GABA), glutamate (Glu), histamine (His), and from receptors with as yet unidentified ligands. The invertebrate organisms in this list are: *Aplysia californica* (a mollusc), the fruit fly *Drosophila melanogaster* (an arthropod), *Caenorhabditis elegans* (a nematode), *Lymnaea stagnalis* (a mollusc), *Capitella capitata* (an annelid), *Schistosoma mansoni* and *S. haematobium* (two human parasitic platyhelminths), and *Helobdella robusta* (an annelid). **b,** Macroscopic current–voltage (*I–V*) relationships recorded under KCl-dilution conditions (solutions 8 and 9 in Supplementary Table 1; pH 7.4, both sides) in the outside-out

configuration, as indicated in Supplementary Fig. 9 and in Methods. The equilibrium (Nernst) potentials at 22°C, using ion concentration values, are −55.0 mV for K^+ and +50.6 mV for Cl^-. Reversal potentials are indicated.

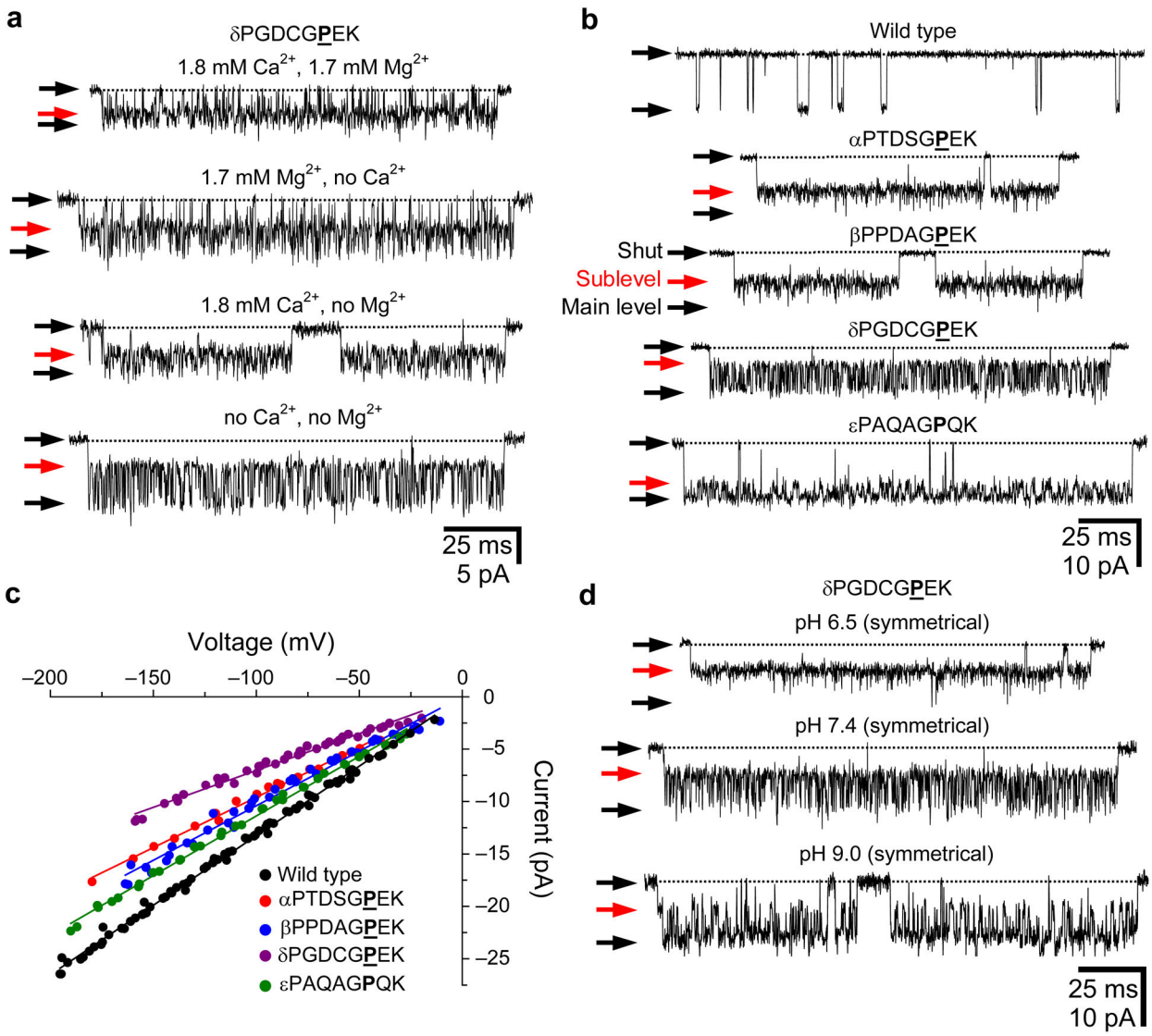

Figure 2. A proline mutation unveils a proton-binding site

a, Single-channel inward currents (cell-attached configuration; ~ −100 mV; 1 μM ACh; $pH_{pipette}$ 7.4) recorded from a mutant AChR having a proline inserted between positions −2′ and −1′ of the δ subunit. To increase the number of main-level ⇄ sublevel interconversions, a mutation that prolongs the mean duration of bursts of openings (εT264P) was also engineered. Solution compositions are indicated in Supplementary Table 1 (solutions 1–3). Mutations are indicated on the M1–M2 loop sequences; underlined bold symbols denote insertions whereas bold symbols (without the underline) denote substitutions. **b,** Inward currents (cell-attached configuration; ~ −100 mV; 1 μM ACh; $pH_{pipette}$ 7.4; solutions 2 and 3) recordedfrom the indicated AChR constructs. The burst-prolonging mutation was εT264P (in the case of AChRs with a proline inserted in the α1, β1 or δ subunit) or δS268Q (in the case of the glycine-to-proline substitution mutant at position −2′ of the ε subunit). In the case of the α1-subunit insertion, the trace shown corresponds to the construct having only one of the two α subunits mutated. **c,** Single-channel *I–V* relationships (cell-attached

configuration; 1 μM ACh; $pH_{pipette}$ 7.4; solutions 2 and 3) recorded from the five constructs in **b**. For clarity, only the *I–V* curves corresponding to the sublevel are shown for the mutants. To facilitate the visual comparison of the slopes, each curve was displaced along the voltage axis so that it extrapolates exactly to the origin. **d,** pH dependence of the main-level ⇄ sublevel current fluctuations (outside-out configuration; −100 mV; 1 μM ACh; solutions 4 and 5).

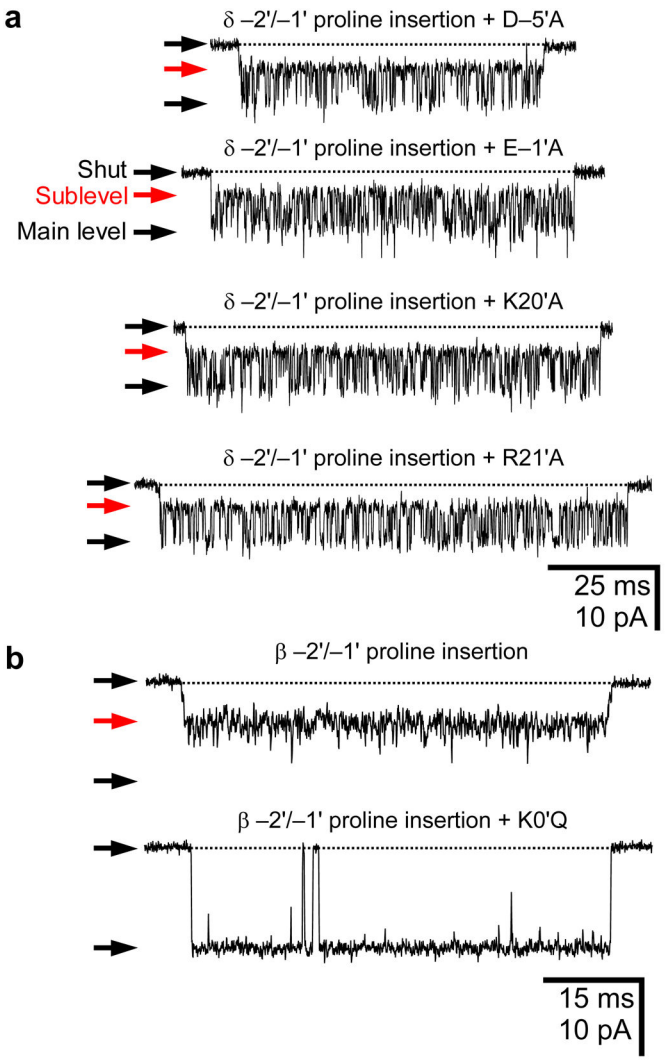

Figure 3. The side chain of the 0′ basic residue is the proton-binding site

a, Single-channel inward currents (cell-attached configuration; 1 μM ACh; $pH_{pipette}$ 7.4; solutions 2 and 3) recorded from AChRs with a proline inserted between positions −2′ and −1′ of the δ subunit and having four of the five native ionizable residues that flank δM2 mutated to alanine, one at a time. The burst-prolonging mutation was εT264P. Mutation of the fifth residue (the 0′ lysine) to alanine, glutamine or valine (in the presence of the inserted proline) abolishes receptor expression on the plasma membrane, as revealed by the lack of specific α-bungarotoxin binding. The applied potential was ~ −100 mV for all constructs, with the exception of the receptor containing the glutamate-to-alanine mutation at position −1′, in which case the potential was ~ −150 mV (to compensate for its lower single-channel conductance). **b**, Inward currents recorded from a mutant AChR having a proline inserted between positions −2′ and −1′ of the β1 subunit and from the mutant having, in addition, a lysine-to-glutamine mutation at position 0′ of the same subunit. The applied potential was ~ −100 mV. All other experimental conditions were as in **a**.

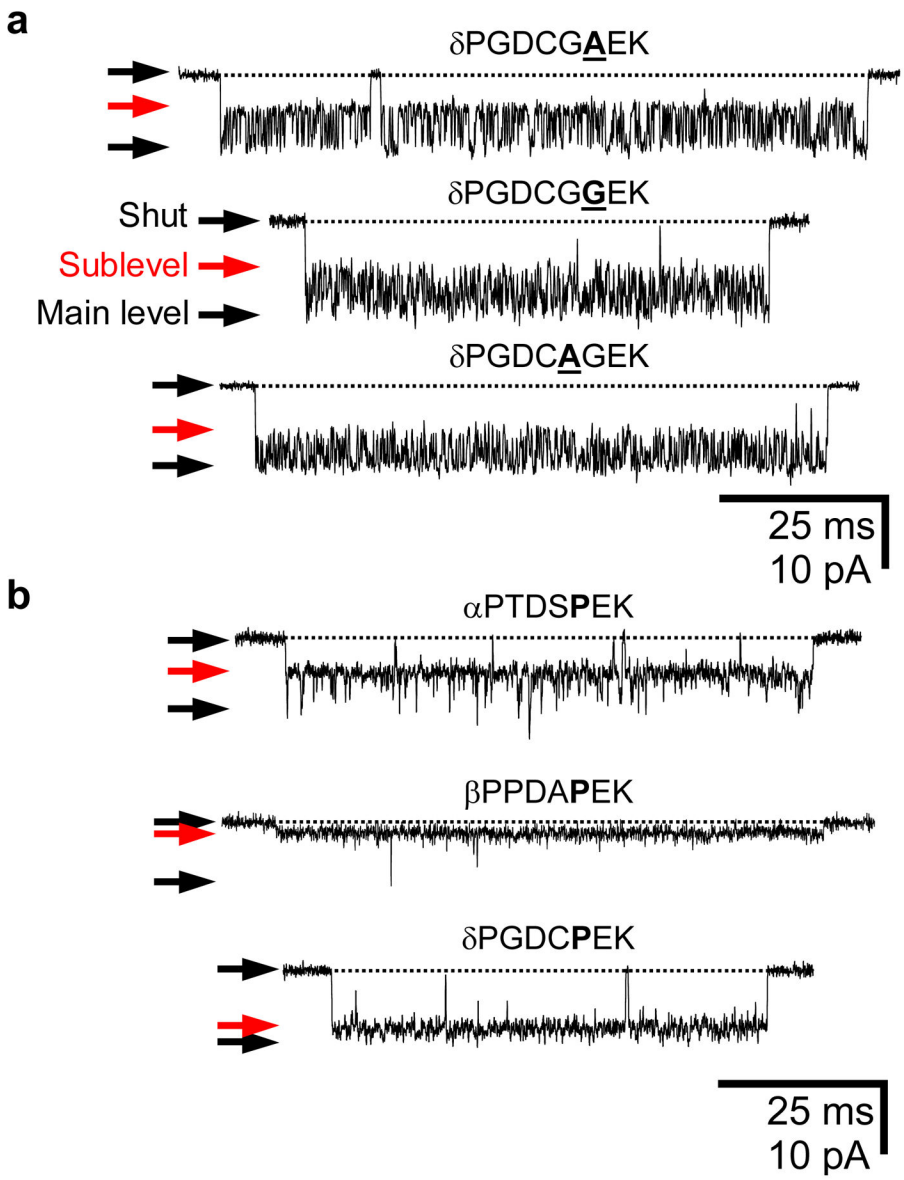

Figure 4. Not only prolines, not only insertions

a, Single-channel inward currents (cell-attached configuration; ~ −100 mV; 1 μM ACh; $pH_{pipette}$ 7.4; solutions 2 and 3) recorded from the indicated AChR insertion mutants. The burst-prolonging mutation was εT264P. Threonine insertions have a similar effect. **b,** Inward currents recorded from the indicated AChR substitution mutants under the same experimental conditions as in **a.** Note that the insertion of a residue is not required to reveal a proton-binding site. Instead, replacing the conserved glycine at position −2′ with a variety of other residues (see Supplementary text; only proline is shown, here) also unveils a protonation site in the four types of subunit. In the case of the α1-subunit mutant, the trace shown corresponds to the construct having only one of the two α subunits mutated. The trace illustrating the effect of a glycine-to-proline mutation at this position of the ε subunit is shown in Fig. 2b.